# Theoretical Analysis and Experimental Research on the Pressing Force of Robot Drilling CFRP Sheet

**Pengqiang Fu** ( pqfu2002@163.com )
Harbin University of Science and Technology https://orcid.org/0000-0002-0246-7881
**Yan Wang**
**Yuhang Miao**
**Yiwen Wang**
**Lijie Zhou**
**Sisi Yang**

**Research Article**

**Keywords:** Robot drilling, End effector, Press foot device, Pressure force, Numerical simulation

**Posted Date:** February 11th, 2022

**DOI:** https://doi.org/10.21203/rs.3.rs-1241162/v1

# Theoretical Analysis and Experimental Research on the Pressing Force of Robot Drilling CFRP Sheet

Pengqiang Fu[1,2*], Yan Wang[1,2], Yuhang Miao[1,2], Yiwen Wang[1,2], Lijie Zhou[1,2], Sisi Yang [3]

1.Key Laboratory of Advanced Manufacturing and Intelligent Technology, Ministry of Education, Harbin University of Science and Technology, Harbin, 150080, P.R. China; pqfu2002@163.com; 857124391@qq.com; 125703044@qq.com; 13946030110@126.com; ajie01265360@sina.com; 2. School of Mechanical and Power Engineering, Harbin University of Science and Technology, Harbin, 150080, P.R. China; 3. Qiqihar Technician College, Qiqihar, 161002, P.R. China; 839063442@qq.com

* Correspondence; pqfu2002@163.com

**Abstract**: In the process of drilling CFRP sheets by industrial robots, the contact stiffness between the terminal actuator and the sheet is poor, which causes the hole position to vibrate during processing. The design of a presser foot device in front of the terminal actuator can effectively solve this problem. The Navier method is used to solve the allowable range of the pressing force of the presser foot. A numerical simulation model for drilling CFRP sheets is established, and the influence of different pressing forces within the allowable range on the drilling quality is studied, and the recommended value of the pressing force of the presser foot is obtained. Drilling experiments are carried out under different pressing forces. The experimental results show that the optimized pressing force of the presser foot can effectively reduce the vibration of the CFRP sheet during the drilling process, and the surface roughness of the drilling hole wall can reach 1.8μm. At the same time, the surface morphology at the exit of the machined hole is improved.

**Key words:** Robot drilling; End effector; Press foot device; Pressure force; Numerical simulation

## 0 Introduction

CFRP (carbon fibre reinforced composite) is increasingly being used as the main structural material for aircraft skins due to its high strength, corrosion resistance and light weight. The physical characteristics of the CFRP itself have an anisotropy result in a metal material that is different from the same-sex, and therefore, in the process of drilling CFRP, stabilizing high quality drilling has become a key issue that needs to be solved, and the aviation manufacturing The quality requirements of the connecting holes are very strict, this requirement to increase the difficulty of drilling CFRP[1]. According to statistics, 70% of the aircraft body fatigue fails is caused by its structural members, and the fatigue crack of the structural member is produced at the connection hole, so the drilling quality has a crucial impact on the life of the aircraft[2-4].

With the arrival of industrial 4.0 and intelligent era, robot automatic drilling technology is applied to the field of aircraft manufacturing and assembly, how to effectively improve the quality of drilling has become one of the focus of domestic and foreign scholars. The skin, as the main structural part of the aircraft wall panel, is usually composed of thin-walled parts. In the process of robotic drilling of thin-walled parts,

the thin-walled parts are subjected to large axial cutting loads that produce elastic deformation and vibration, ultimately leading to poor drilling quality[5-6]. For such problems, scholars Olsson[7], von[8] for improving contact stiffness between terminal actuators and workpieces to design a rigid presser foot before the terminal actuator to suppress the vibration of the hole position during drilling, and EI[9] The MFEE developed by the company uses pneumatic manner to press the presser foot to reduce the vibration of the workpiece during the drilling process. Although some scholars have verified in drilling experiments that compression force can suppress workpiece vibration when drilling thin-walled parts, thus improving the quality of surface roughness and cylindricity of the hole, but the compression force used for CFRP thin plate is still less research[10]. The size of the pressing force is a problem[11], the pressing force is too small to eliminate the vibration of the workpiece, and the pressing force is too large to cause the workpiece to produce severe deformation or even cracks. Therefore, there is an urgent need to eliminate vibrations in the workpiece during machining without the compression force causing severe deformation and cracking in the sheet.

To address the above issues, this paper uses a robot and a special end-effector for drilling thin CFRP sheets as a platform, the allowable range of compression force can be worked out by analytical method, the finite element simulation model of drilling CFRP sheet is established, revealing the regular of influence of different compression forces on drilling quality, the optimized compression force parameter value is obtained, and experimental verification was carried out.

# 1 Action principle of presser foot pressing force of robot drilling terminal actuator

## 1.1 Drilling end-effector

The drilling end-effector is connected to the robot via a quick-change flange and is mounted on the end of the robot. The structure of the drilling terminal actuator XNZF01 designed in this paper is shown in Fig.1, it consists of five main components: spindle unit, feed unit, clamping unit, vision unit and normal detection unit. The spindle is infinitely variable, with a maximum speed of 9,000 r/min. The feed movement is driven by servo motors driving high-precision ball screws mounted on the actuator frame. The servo motor is connected to a high precision ball screw via a flexible coupling to precisely position the tool relative to the workpiece and perform the machining feed.

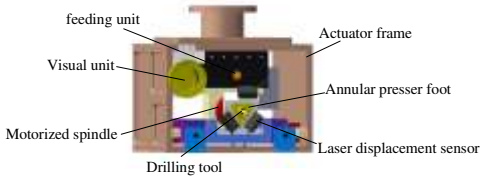


Fig.1 Drilling end-effectors

## 1.2 Pressing device

The main structure of the pressing device is integrated in the front end of the terminal actuator, as shown in Fig.2. Four sheet metal members are used to fix the cylinders on the left and right sides. During operation, the cylinder pushes the structural components connected above the slider to provide linear displacement. Its moving direction is parallel to the feed direction. The moving distance is limited by the mechanical limit installed on the actuator frame. The annular presser foot is in direct contact with the workpiece and provides pressing force,

as shown in Fig.3, it is secured to the structural components attached above the slider by hexagonal bolts.

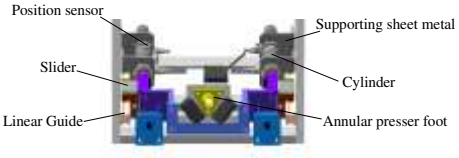


Fig.2 Compression device

Fig.3 Annular presser foot

## 1.3 Action principle of presser foot pressing force

In the process of drilling thin-walled parts, the thin-walled parts will be subjected to large axial load, This lead to thin-walled parts will lead to different degrees of vibration along the tool axis. The greater the tool feed speed, the greater the amplitude. As a one-way pressing device used in robot automatic drilling, the presser foot is mainly used to reduce the vibration of the workpiece in the processing process. Its action principle is shown in Fig.4. Although the presser foot can reduce the vibration of the workpiece along the hole when machining thin-walled parts, it is a difficult problem to apply the magnitude of the pressing force. The pressing force is too small, the effect of restraining workpiece vibration during processing is poor, and the hole inlet and outlet continuously shrink and expand, resulting in the increase of hole wall surface roughness. If the pressing force is too large, the sample will produce large deformation before machining, resulting in the increase of instantaneous rebound amplitude after drilling, which will bring greater vibration and noise[12]. For carbon fiber composites, matrix cracks are easy to occur when the bending deformation exceeds 0.3 mm. Matrix crack propagation will lead to weak interlayer bonding and even brittle fracture of composites, which will seriously affect the drilling quality[13]. It is therefore crucial to solve for the permissible range of compression forces.

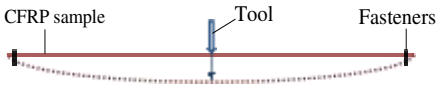


(a) Drilling without presser foot

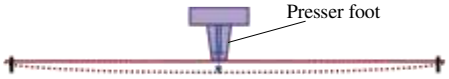


(b) Drilling with presser foot

Fig.4 Action principle diagram of presser foot pressing force

# 2 Solving for the permissible range of Presser foot pressing force

## 2.1 Drilling end-effector

Taking the vertical wall panel of aircraft tail as an example, its local curvature to be machined is small, so the surface of the vertical sample to be machined can be regarded as a flat plate. Its four sides are fixed with special clamps, which limits x, y, Z and four degrees of freedom rotating around the Z axis in three-dimensional space, so it can be regarded as a simple support. Assuming that the length of the sample is a, the width is B, the thickness is h, the axial force during drilling is fa, the pressing force of the presser foot is evenly distributed on the sample, and the pressure is Pb, and the inner and outer radii of the presser foot acting on the sample are R and R respectively, force conditions of the sample during processing is shown in Fig.5.

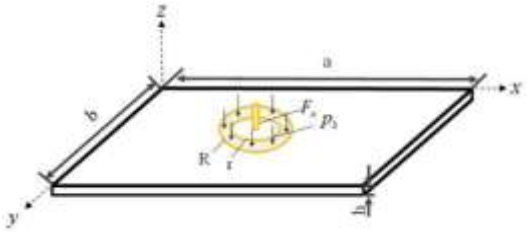

Fig.5 Schematic diagram of forces during sample processing

Since the pressing force action area of the presser foot and the drilling axial force action area are very small relative to the sample area, the radius around the center of the presser foot be $R_1=(R+r)/2$ , The uniformly distributed linear load with pressure P represents the pressing force[14]. The drilling axial force acts on the presser foot center, the simplified force diagram is shown in Fig.6.

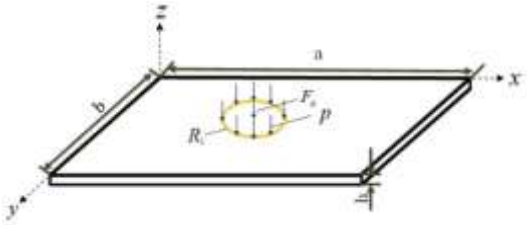

Fig.6 The simplified force diagram

## 2.2 Navier method to calculate the allowable range of compression force

The critical bending boundary value of CFRP thin plate is solved by Navier method, first, the deflection ω Expressed as trigonometric series:

$$\omega=\sum_{m=1}^{\infty}\sum_{n=1}^{\infty}A_{mn}\sin\frac{m\pi x}{a}\sin\frac{n\pi y}{b} \tag{1}$$

In order to seek the deflection $\omega$ of general solution, It needs to be substituted the differential equation of elastic surface of thin plate:

$$D\nabla^4\omega=\mathrm{q}(x,y) \tag{2}$$

$$\nabla^4\omega=\frac{\partial^4\omega}{\partial x^4}+2\frac{\partial^4\omega}{\partial x^2\partial y^2}+\frac{\partial^4\omega}{\partial y^4} \tag{3}$$

Where D is the bending stiffness, and its expression is:

$$D=\frac{Ec^3}{12(1-\upsilon^2)} \tag{4}$$

Deflection $\omega$ Substitute into the differential equation of elastic surface to obtain:

$$\frac{\mathrm{q}(x,y)}{D}=\pi^4\sum_{m=1}^{\infty}\sum_{n=1}^{\infty}A_{mn}\left(\frac{m^2}{a^2}+\frac{n^2}{b^2}\right)^2\sin\frac{m\pi x}{a}\sin\frac{n\pi y}{b} \tag{5}$$

In order to solve $A_{mn}$, surface load $q(x,y)$ can be expanded into trigonometric series of the same form. After simplification, $A_{mn}$ can be obtained by combining with the above formula:

$$A_{mn}=\frac{4\int_0^a\int_0^b\mathrm{q}(x,y)\sin\frac{m\pi x}{a}\sin\frac{n\pi y}{b}dxdy}{\pi^4abD\left(\frac{m^2}{a^2}+\frac{n^2}{b^2}\right)^2} \tag{6}$$

Then the deflection function of simply supported template on four sides ω The general solution can be expressed as:

$$\omega=\sum_{m=1}^{\infty}\sum_{n=1}^{\infty}\frac{4\int_0^a\int_0^b\mathrm{q}(x,y)\sin\frac{m\pi x}{a}\sin\frac{n\pi y}{b}dxdy}{\pi^4abD\left(\frac{m^2}{a^2}+\frac{n^2}{b^2}\right)^2}\sin\frac{m\pi x}{a}\sin\frac{n\pi y}{b} \tag{7}$$

Let the coordinates of the drilling axial force acting on the CFRP template be (x0, Y0), The simplified relationship between the pressing force radius of the presser foot and the axial force coordinate in 2.1 is used as the parameter equation ( $x_0+R_1\cos\theta$, $y_0+R_1\sin\theta$ ), $0\le\theta\le2\pi$ indicates. When the template is jointly acted by the drilling axial force and pressing force, the deflection formula of any point (x, y) in the template is:

$$\omega=\frac{4F_a}{\pi^4abD}\sin\frac{m\pi x}{a}\sin\frac{n\pi y}{b}\sum_{m=1}^{\infty}\sum_{n=1}^{\infty}\frac{\sin\frac{m\pi x_0}{a}\sin\frac{n\pi y_0}{b}}{\left(\frac{m^2}{a^2}+\frac{n^2}{b^2}\right)^2}+\sin\frac{m\pi x}{a}\sin\frac{n\pi y}{b}\times$$
$$\frac{4p}{\pi^4abD}\sum_{m=1}^{\infty}\sum_{n=1}^{\infty}\frac{\int_0^{2\pi}\mathrm{R}_1\sin\frac{m\pi(x_0+\mathrm{R}_1\cos\theta)}{a}\sin\frac{n\pi(y_0+\mathrm{R}_1\sin\theta)}{b}d\theta}{\left(\frac{m^2}{a^2}+\frac{n^2}{b^2}\right)^2} \tag{8}$$

The internal moment of force is:

$$M=\sqrt{(M_x)^2+(M_y)^2} \tag{9}$$

Where MX and my are the internal moment of force in X direction and Y direction respectively, and their expressions are:

$$\begin{cases} M_x = \int_{-c/2}^{c/2} \delta_x u du = -D\left(\dfrac{\partial^2 \omega}{\partial x^2} + \upsilon \dfrac{\partial^2 \omega}{\partial y^2}\right) \\ M_y = \int_{-c/2}^{c/2} \delta_y u du = -D\left(\dfrac{\partial^2 \omega}{\partial y^2} + \upsilon \dfrac{\partial^2 \omega}{\partial x^2}\right) \end{cases} \quad (10)$$

In this paper, T800 CFRP sample is selected as the experimental workpiece, with length a = 200 mm, width b = 28 mm, thickness h = 3.6 mm, average elastic modulus E of 294 GPA and Poisson's ratio υ= 0.3, allowable bending strength[ σ] The approximate value is 780 MPa. The internal and external radii r and R of the presser foot are 8 mm and 12 mm respectively, then R1 = (R + r) / 2 = 10 mm. The axial force of composite drilling is usually much less than that of metal, and $F_a$ can be taken as 200 N[15]. The allowable internal force moment can be obtained according to the following formula:

$$[M] = \int_{-c/2}^{c/2} \frac{[\sigma]}{c} s^2 ds \quad (11)$$

Find [M] ≈ 867 n.mm. Taking the center point of the template as an example, substitute it into formula (8) to obtain the specific expression of the deflection at this point:

$$\omega = \sin\frac{m\pi x}{a}\sin\frac{n\pi y}{b}\frac{4F_a}{\pi^4 abD}\sum_{m=1}^{\infty}\sum_{n=1}^{\infty}\frac{\sin\frac{m\pi}{2}\sin\frac{n\pi}{2}}{\left(\frac{m^2}{a^2}+\frac{n^2}{b^2}\right)^2} + \sin\frac{m\pi x}{a}\sin\frac{n\pi y}{b}\times \frac{4p}{\pi^4 abD}\sum_{m=1}^{\infty}\sum_{n=1}^{\infty}\frac{\int_0^{2\pi} \mathrm{R}_1 \sin\frac{m\pi\left(\frac{a}{2}+\mathrm{R}_1\cos\theta\right)}{a}\sin\frac{n\pi\left(\frac{b}{2}+\mathrm{R}_1\sin\theta\right)}{b} d\theta}{\left(\frac{m^2}{a^2}+\frac{n^2}{b^2}\right)^2} \quad (12)$$

Then substitute it into formula (10) to obtain the internal moment of the center point in X direction and Y direction, which are respectively:

$$\begin{cases} M_x = 0.0131p + 105.5 \\ M_y = 0.0162p + 116.7 \end{cases} \quad (13)$$

Obtain Internal closing moment is:

$$M = \sqrt{4.3405\times10^{-4}p^2 + 6.54518p + 24749.14} \quad (14)$$

Theoretically $[M] \le M$, so the allowable pressing force F of the presser foot can be solved $F_s \le [F_s] = 2\pi R_1 p \approx 850$ N。That is, when the pressing force of the presser foot does not exceed 850 N, the CFRP sample will not produce matrix cracks due to excessive bending deformation[16]. Due to the slow convergence speed of Navier trigonometric series solution process, it is impossible to select infinite items in calculation. The obtained linear load p is the approximate solution. In practical application, 850 N can be regarded as the allowable value range of compression force.

When the sample size and material change, the allowable value range of the corresponding pressing force can be obtained by referring to the above method.

# 3 Numerical simulation

Based on the allowable range of compression force, the finite element model of drilling CFRP thin plate is established through the finite element software ABAQUS, and the influence of different compression force on drilling quality within the allowable range is further analyzed.

## 3.1 Finite element modeling

The finite element model of drilling CFRP sample in this paper is shown in Fig.7. The displacement of the sample in the X and Y directions is limited by the fixture. The tool diameter is 6 mm, the front angle is 130° and the rear angle is 12°, and is set as rigid. The length, width, thickness and pressing force action area of the model are consistent with the sample. The total number of elements included in the tool and CFRP sample after meshing is 23469 and 209532 respectively. The model refines the mesh around the drilling area to ensure the simulation accuracy and efficiency. Four reference points are set in the whole

model. Reference point 1 acts on the tool to output the drilling axial force results, and reference points 2, 3 and 4 act around the drilling area to output the sample amplitude results. The single layer thickness of CFRP unidirectional laminate is about 0.33 mm, a total of 10 layers, and the fiber direction angle is 0°. Before its failure, it is simulated as anisotropic elastic material, and the material constitutive model is established by VUMAT subroutine. Adding adhesive layer cohesive element between CFRP solid element layers, coheisive interface element adopts 8-node three-dimensional adhesive element (coh3d8), and CFRP solid element adopts 8-node linear hexahedron element and reduced integral, which can effectively improve the accuracy of modeling.

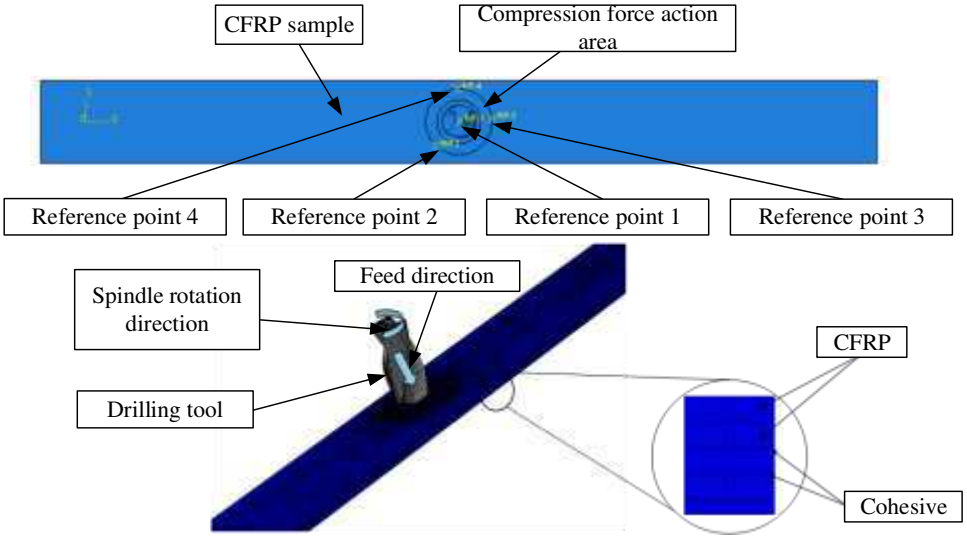


Fig.7 Finite element model of drilling CFRP template

## 3.2 Parameter setting

In order to ensure the accuracy of the finite element simulation calculation, the mechanical parameters of T800 grade CFRP unidirectional laminates used in the numerical simulation are consistent with those used in the experiment. See Table 1 for some mechanical properties of CFRP unidirectional laminates used in the experiment. The unidirectional CFRP layer is simulated as an equivalent homogeneous material with anisotropic characteristics, and the damage initiation criterion is based on Hashin theory. The cohesive layer is located between two continuous layers. When the normal stress exceeds the stress limit, the interface element fails. In this study, the quadratic nominal stress criterion (quads damage) is used as the damage initiation criterion of the cohesive element, as shown in formula (15), the element properties of the cohesive element are shown in Table 2, and the process parameters used for drilling simulation are shown in Table 3.

$$\left\{\frac{\langle t_n \rangle}{t_n^0}\right\}^2+\left\{\frac{t_s}{t_s^0}\right\}^2+\left\{\frac{t_t}{t_t^0}\right\}^2=1 \qquad (15)$$

## 3.3 Result analysis

### *3.3.1 Drilling process*

The numerical simulation of the entire drilling state process is divided into three steps, namely just drilling, drilling in progress and after drilling, and the results of the simulation are shown in Fig.8.

Table 1 mechanical parameters of CFRP laminates

| Properties | $E_1$(GPa) | $E_2$(GPa) | $G_{12}$(GPa) | $\gamma_{12}$ | $\rho$(kg/m$^3$) |
|---|---|---|---|---|---|
| Value | 230 | 14 | 28 | 0.3 | 1760 |
| Properties | $X^T$(MPa) | $X^C$(MPa) | $Y^T$(MPa) | $Y^c$(MPa) | S(MPa) |

| Value | 3530 | 1800 | 350 | 2730 | 380 |
|---|---|---|---|---|---|

Table 2 parameters of coherent unit

| Parameter | $\rho$(kg/cm$^3$) | $E_{nn}$ | $E_{ss}$= $E_{tt}$ | $t_t^0$ | $t_s^0 = t_t^0$ | $G_{Ic}$ |
|---|---|---|---|---|---|---|
| Value | $4.0\times10^{-9}$ | 40GPa | 10Gpa | 60MPa | 90MPa | $280J/m^2$ |

Table 3 simulation process parameters

| d/mm | Rotating speed(r/min) | Feed rate(mm/min) | Fs/N |
|---|---|---|---|
| 6 | 3000 | 90、150、210 | 0、250、550、850 |

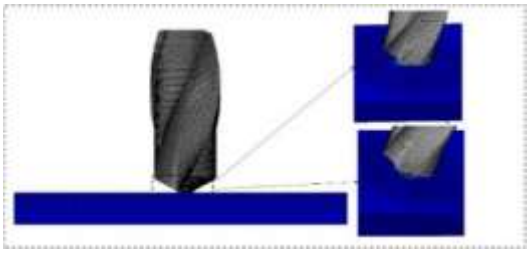

(a) Just drilling

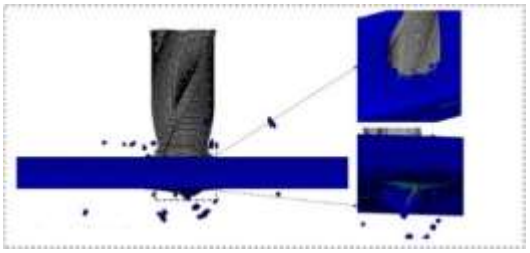

(b) Drilling in progress

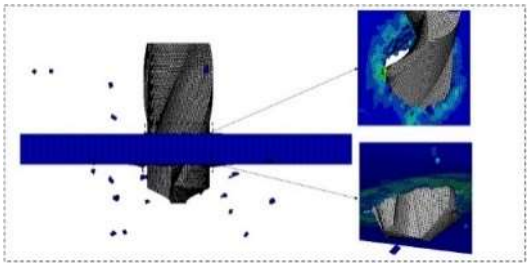

(c) after drilling

Fig. 8 simulation process of drilling CFRP sheet

It can be seen from Fig.8(a) that when just drilling, the drill tip is in direct contact with the CFRP sheet, and the sheet has serious elastic deformation due to the extrusion of the drill tip. With the cutting of the drill bit, the extrusion energy generated by the drill tip and the sheet is released to the CFRP matrix, and the elastic deformation gradually decreases, at this time, the fibers with weak fiber matrix bonding strength peel off from the matrix and begin to form cuttings. During the drilling process, as shown in Fig.8(b), the cuttings gradually increase, while the macro chip size of CFRP is usually in the micron level. The formation of simulated chips is related to the grid size and failure displacement. The single grid of this model is about 105 μm～230 μm Therefore, the macro model of drilling CFRP samples established does not form long strip and C-type cuttings with a size of more than 1 mm. After drilling, as shown in Fig.8(c), more fine ribbon fiber debris detritus on the surface of the sample. After processing, the outlet and inlet surfaces are relatively neat.

In the dynamic simulation process with feed speed of 90 mm/min and compression force of 850 N, the stress nephogram of CFRP template at different times is shown in Fig.9. It can be seen that in the whole numerical simulation process, the CFRP samples outside the drilling area do not produce large stress. Therefore, the samples outside the drilling area will not have fiber separation and fracture during the drilling process.

***3.3.2 Drilling area amplitude***

In the drilling process, the CFRP template is limited by four sides and there is no other force in X and Y directions. Therefore, it is only necessary to analyze the displacement change in Z direction in the drilling area[17]. The three reference points set in the drilling area reflect the vibration and deformation of the drilling area. In the simulation results, there is no significant difference in the z-direction displacement of the three reference points, so one of them is taken for analysis. When the feed speed is 90 mm/min and the sampling frequency is 1 kHz, four different compression

forces act on the sample. The z-direction vibration simulation results of the reference point are shown in Fig.10.

From the simulation results in Fig.10, it can be seen in drilling that the vibration degree of the drilling area in the Z direction is related to the value of the pressing force of the presser foot. When the pressing force is 0 N, during the drilling process from 0.2 s to 2.6 s, the sample is only subjected to the drilling axial force in the Z direction. Therefore, the deformation $D_f$ in the Z direction of the drilling area at the beginning of drilling is small, with a value of 0.08 mm, but the amplitude in the drilling area is large, and the maximum amplitude $S_{max}$ is

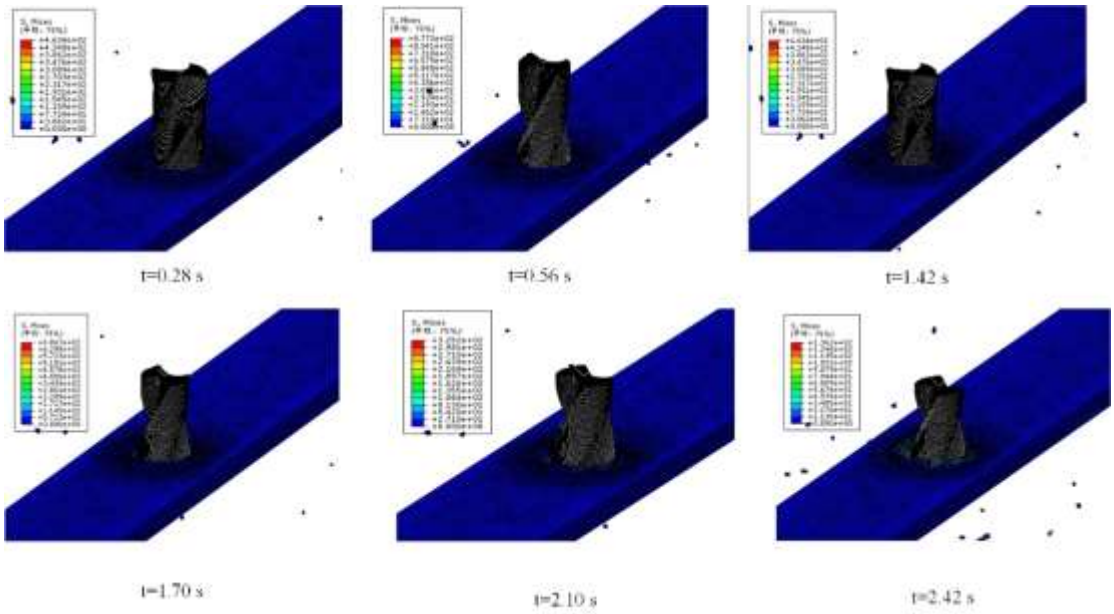


Fig. 9 stress nephogram of CFRP sample at different times

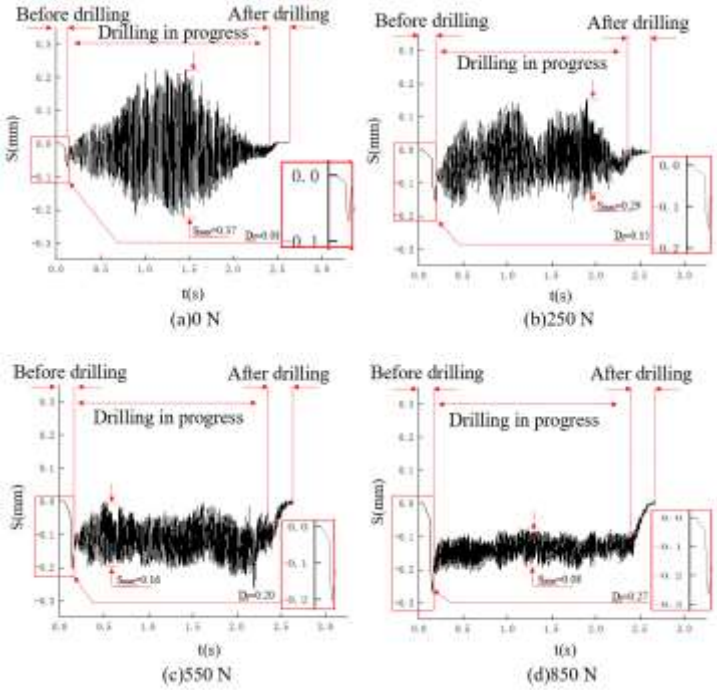


Fig. 10 vibration in Z direction of drilling area

0.37 mm. As the pressing force increases to 850 n, the deformation in the drilling area increases continuously at the beginning of drilling, and the maximum deformation $D_f$ reaches 0.27 mm, which is due to the joint action of the pressing force and the drilling axial force at the beginning of drilling. However, as the pressing force increases, the amplitude generated in the drilling area decreases continuously during drilling. At 850 n, the maximum amplitude $S_{max}$ is only 0.08 mm. If the pressing force is continuously increased, the bending deformation of the sample will exceed 0.33 mm before drilling, which will produce matrix cracks. During drilling, the matrix cracks will continue to expand, resulting in brittle fracture.

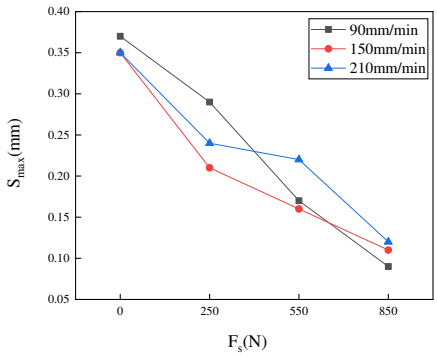


Fig. 11 variation trend of maximum amplitude with pressing force

Considering the different variation degree of amplitude in the drilling time, the maximum displacement of the sample in this time period. the maximum amplitude Smax, is taken to represent the amplitude of the drilling area in the feed direction of the main shaft. When the feed speed is different, the result of the increase of the maximum amplitude with the pressing force is shown in Fig.11. It can be seen from Fig.11 that the maximum amplitude of CFRP sample has a great correlation with the compression force, and the overall trend is to decrease with the increase of compression force. When the pressing force is 850 N, the maximum amplitude under different feed rates reaches the lowest, the sample amplitude in the drilling process is the lowest, and the hole wall quality is the highest.

### *3.3.3 Drilling axial force*

In the dynamic simulation of spindle speed 3000 R / min, feed speed 210 mm / min and pressing force 0 N, it is obtained that the average drilling axial force $F_m$ is 159.7 N and the maximum drilling axial force $F_{max}$ is 198.0 n. When other parameters remain unchanged and the pressing force is increased to 850 n, the average drilling axial force $F_m$ is 122.4 N and the maximum drilling axial force $F_{max}$ is 172.0 N. In the whole simulation process, when the feed speed is 90 mm / min and the pressing force is 850 N, the average drilling axial force reaches the lowest value of 77.3 N. Fig.12 shows the relationship between the average drilling axial force $F_m$ and the pressing force $F_s$ at different feed speeds.

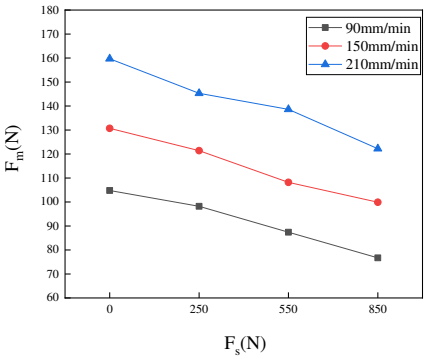


Fig. 12 relationship between average drilling axial force FM and pressing force FS

As can be seen from Fig.12, the drilling axial force decreases gradually with the increase of the pressing force. For CFRP workpiece, the main reason for its surface tear defect is the drilling axial force. Reducing the drilling axial force can effectively inhibit its surface tear defect[18]. Therefore, through simulation analysis, when the pressing force of the presser foot is 850 N, the drilling axial force is the smallest and the drilling surface quality is the highest.

# 4 Drilling experiment

## 4.1 Experimental condition

In order to verify the influence of the pressing force of the presser foot on the drilling quality and the correctness of the simulation results, a robot drilling system as shown in Fig.13 is built.

The robot drilling system shown in Fig.13 includes robot (FANUC robot R-2000ic / 165F), drilling terminal actuator, dynamometer (Kistler 9257b), CFRP sample, upper computer, etc. In the experiment, 6 mm carbide coated twist drill was used as the cutting tool, with a

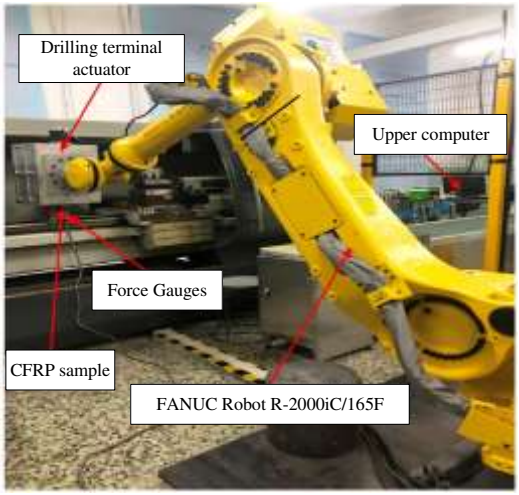


Fig. 13 experimental bench for robot drilling CFRP sheet

front angle of 130° and a back angle of 12°. The T800 unidirectional laminated template with a fiber direction angle of 0° was selected for CFRP sheet, with a size of 200 mm × 28 mm × 3.6 mm。 The drilling terminal actuator is integrated into the end flange of the robot. During the experiment, the robot drives the drilling actuator to the target pose, and the feed unit feeds and carries out the drilling experiment.

## 4.2 Experimental result

### *4.2.1 Axial force results*

Using the parameters in Table 4, the drilling axial force measurement experiment is carried out with Kistler 9257b. When the spindle speed is 3000 R/min, the feed speed is 210 mm/min, and the pressing force is 0 N, the average axial force measured is 151.3 N, and the maximum drilling axial force is 191.4 N. The variation curve of drilling axial force measured experimentally with time is shown in Fig14. When other parameters remain unchanged and the pressing force is increased to 850 N, the average drilling axial force $F_m$ is 125.6 N and the maximum drilling axial force $F_{max}$ is 162.0 N. The maximum drilling axial force calculated by simulation and the maximum drilling axial force measured actually do not exceed 200 N, which proves that it is reasonable to take 200 N as the drilling axial force when calculating the allowable range of pressing force.

Table 4 Experimental drilling parameters

| Hole serial number/ H | n/ $(r.\min^{-1})$ | V/ $(mm.\min^{-1})$ | $F_s$/ (N) |
|---|---|---|---|
| 1-1 | 3000 | 90 | 0 |
| 1-2 | 3000 | 90 | 250 |
| 1-3 | 3000 | 90 | 550 |
| 1-4 | 3000 | 90 | 850 |
| 2-1 | 3000 | 150 | 0 |
| 2-2 | 3000 | 150 | 250 |
| 2-3 | 3000 | 150 | 550 |
| 2-4 | 3000 | 150 | 850 |
| 3-1 | 3000 | 210 | 0 |
| 3-2 | 3000 | 210 | 250 |
| 3-3 | 3000 | 210 | 550 |
| 3-4 | 3000 | 210 | 850 |

The comparison of experimental and simulated drilling axial force data is shown in Fig.15. It can be seen from Fig.15 that there is a certain error between the maximum drilling axial force $F_{max}$ and the average drilling axial force $F_m$. The main reasons for this error are as follows: (1) The Hashin model of progressive failure of composites is not perfect; (2) Insufficient mesh refinement; (3) Mesh distortion may occur when the fiber is

separated from the matrix; (4) There are inevitable differences between the simulated boundary conditions and the actual boundary conditions. The above reasons lead to the error of experiment and simulation. The experimental and simulated drilling axial force data are shown in Table 5. It can be seen from Table 5 that the error between the maximum drilling axial force and the average drilling axial force is no more than 10%, which proves that the simulation is still reliable.

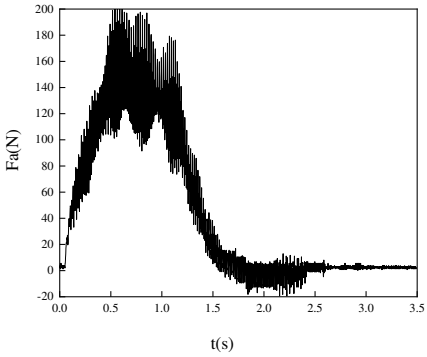


Fig.14 Variation curve of drilling axial force with time

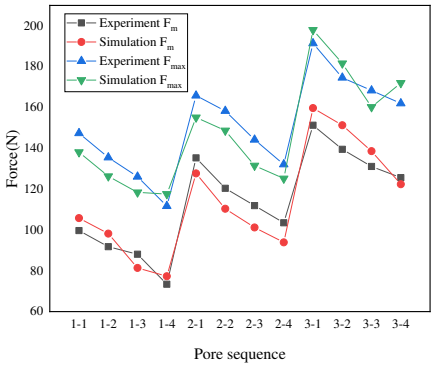


Fig. 15 Comparison of experimental and simulated drilling axial force results

Table 5 Experimental and simulated drilling axial force result data

| Pore sequence | Experiment $F_m$（N） | Simulation $F_m$（N） | Error | Experiment $F_{max}$（N） | Simulation $F_{max}$（N） | Error |
|---|---|---|---|---|---|---|
| 1-1 | 99.7 | 105.8 | -6.12% | 147.4 | 138.1 | 6.31% |
| 1-2 | 91.8 | 98.2 | -6.97% | 135.5 | 126.3 | 6.79% |
| 1-3 | 88.1 | 81.4 | 7.60% | 126.1 | 118.4 | 6.11% |
| 1-4 | 73.4 | 77.3 | -5.31% | 111.7 | 117.6 | -5.28% |
| 2-1 | 135.3 | 127.7 | 5.62% | 165.8 | 155.1 | 6.45% |
| 2-2 | 120.4 | 110.4 | 8.31% | 158.3 | 148.7 | 6.06% |
| 2-3 | 111.9 | 101.2 | 9.56% | 144.2 | 131.5 | 8.81% |
| 2-4 | 103.5 | 93.9 | 9.28% | 132.1 | 125.2 | 5.22% |
| 3-1 | 151.3 | 159.7 | -5.55% | 191.4 | 198.0 | -3.45% |
| 3-2 | 139.5 | 151.3 | -8.46% | 174.6 | 181.6 | -4.02% |
| 3-3 | 131.1 | 138.6 | -5.72% | 168.3 | 160.2 | 4.81% |
| 3-4 | 125.6 | 122.4 | 2.55% | 162.0 | 172.0 | -6.17% |

### *4.2.2 Hole wall roughness comparison*

The surface roughness of the hole wall of the machined hole was observed with a white light interferometer (Taylor Hobson CCI MP). Taking hole 1 as an example, Fig.16 shows the three-dimensional morphology of the hole wall surface of hole 1 when the pressing force is 0 n. It can be seen from the figure that due to the large amplitude of the processing process when the pressing force is 0 N, the hole wall surface is uneven, forming some white and Red areas with high protrusions, and the area of the whole protrusion area is large. When the pressure

tightening force is increased, the amplitude of the processing process decreases, and the area of the surface uneven area and convex area gradually decreases. Fig.17 shows the three-dimensional surface morphology of the hole wall of hole 1 when the pressing force is different.

It can be seen from the figure that when the pressing force is 250 N, the area of the raised red area is greatly reduced compared with that when the pressing force is 0 N, and the surface quality of the hole wall is improved. When the pressing force is increased to 550 N, the raised white area has disappeared, and the surface roughness value of the hole wall is reduced. When the pressing force continues to increase to 850 N, the area of the raised area is the smallest, and the surface roughness value of the hole wall is the lowest, Directly reflected in the relatively smooth hole wall.

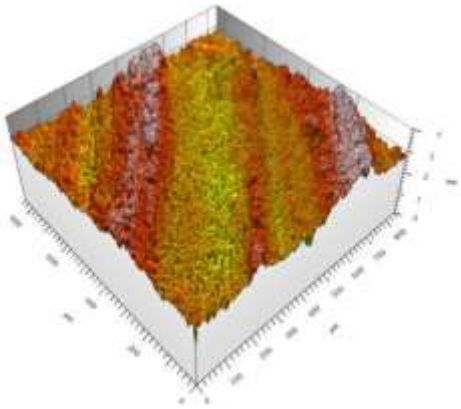

Fig.16 Three dimensional morphology of hole wall surface of hole 1 under compression force of 0 N

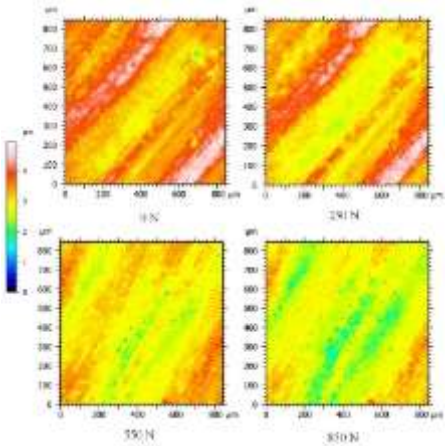

Fig. 17 Three dimensional morphology of hole wall surface of hole 1

After three repeated experiments, the average value of hole wall roughness Ra of machined holes under different pressing forces is shown in Fig.18, and the standard deviation is shown in Fig.19. It can be seen from Fig. 18 that when the pressing force is 0 N, there are many vibration marks on the hole wall of the machined hole, and the average surface roughness of the hole wall of holes 1 ~ 3 is 4.6 ~ 6.3 μm, when the pressing force is increased to 250 n, the hole wall quality of the machined hole is improved to a certain extent, the vibration pattern is gradually reduced, and the average surface roughness of the hole wall of holes 1 ~ 3 is 3.3 ~ 4.6 μm.

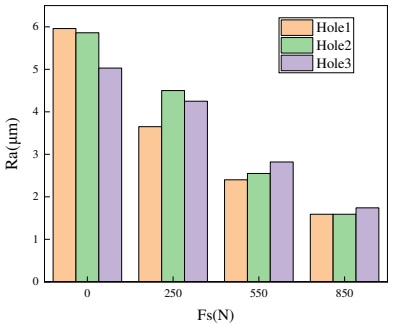


Fig. 18 Mean value of hole wall roughness in three experiments

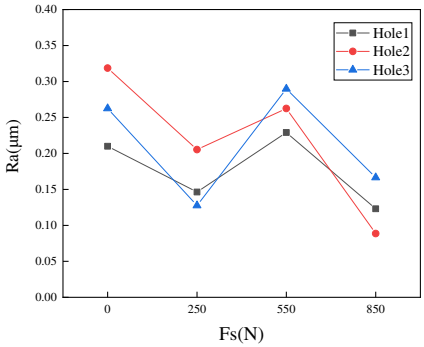


Fig.19 Standard deviation of hole wall roughness

When the pressing force is further increased to 550 N, the hole wall quality of the machined hole is greatly improved, the vibration lines on the hole wall are significantly reduced and the appearance is smooth. The average roughness of the hole wall of holes 1 ~

3 is about 1.8 ~ 3.3 μm. When the pressing force increases to 850 n, the hole wall finish is greatly improved, and the average surface roughness of holes 1 ~ 3 is 1.8 μm within, the minimum value of multiple experiments is 1.58 μm。It can be seen from the results in Fig.19 that the standard deviation of holes 1 ~ 3 is less than 0.35 μm. It shows that the surface roughness of holes 1 ~ 3 obtained from many experiments is close to the average value, and the single experimental data is reliable. Therefore, increasing the high-pressure tightening force within the allowable range of tightening force can significantly improve the hole wall roughness after drilling and effectively improve the drilling quality.

***4.2.3 Comparison of borehole surface defects***

By observing the surface morphology of the machined holes with a super depth of field microscope (KEYENCE vhx-500fe), it can be found that there are no obvious defects at the entrance of the holes. By observing the outlet morphology, it can be found that when the pressing force is 0 N, the outlets of holes 1 ~ 3 have different degrees of tearing defects, among which the tearing defect of hole 3 is the most serious, because under the same pressing force, the larger the feed rate, the greater the drilling axial force, and the main reason affecting the tearing defect is the excessive drilling axial force, Therefore, the tearing defect causing hole 3 is the most serious. When the pressing force is 250N, the tearing defects of holes 1 ~ 3 have been improved to some extent, but the defects are still obvious. With the pressing force increasing to 550 N, there are no obvious tearing defects at the outlet of machined hole 1, and the tearing defects of holes 2 and 3 still exist. However, compared with the pressing force of 0 N, the surface quality of holes 2 and 3 has been greatly improved. When the pressing force is further increased to 850 N, the machined holes 1 ~ 3 have no tear defects. Taking hole 1 as an example, Fig.20 shows the comparison of outlet surface morphology of hole 1 under different pressing forces.

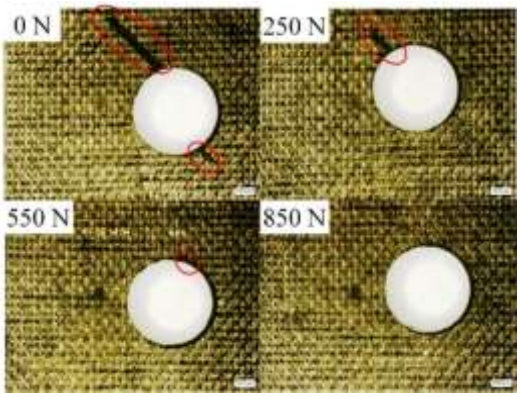


Fig. 20 comparison of outlet morphology of hole 1 under different pressing forces

## 4.3 Results Analysis

According to the analysis of the above experimental results, when the presser foot pressing force is 850 N, the average drilling axial force and the maximum drilling axial force are lower than 0 N, 250 N and 550 N, when the presser foot pressing force is 850 N, the average drilling axial force of holes 1 ~ 3 is about 33.2 N lower than that when the presser foot pressing force is 0 N, and the maximum drilling axial force is 25.4 N lower, The fundamental reason is that the large pressing force suppresses the vibration of CFRP thin plate during drilling, which improves the processing conditions and reduces the drilling axial force.

Compare the quality of the hole after the drilling process, when the pressing force of the presser foot is 850 N, it is greatly improved compared with 0 N, 250 N and 550 N, which is mainly reflected in the better outlet surface morphology and higher hole wall finish. Therefore, under the same processing conditions, the pressing force of the presser foot is close to the upper limit of the allowable range, which can effectively improve the quality of the processed hole.

# 5 Conclusion

(1) By designing a pneumatic presser foot device in front of the end actuator of the industrial robot, effective in suppressing vibrations generated in the hole position when drilling thin CFRP sheets.
(2) The allowable range of presser foot pressing force is 0 ~ 850 N by Navier method.
(3) The process of drilling CFRP thin plate under different pressing force is numerically simulated by finite element method, the influence of different pressing forces on drilling quality within the allowable range of presser foot pressing force is further analyzed, and the optimal value within the allowable range of presser foot pressing force is obtained.
(4) Through the drilling experiment, the drilling quality under different pressing force is compared, verified that the surface roughness of the hole wall can be up to 1.8 μm when drilling with an optimized presser foot pressing force. At the same time, the surface morphology at the outlet of the machined hole can be improved.

**Funding** This study was funded by the National Natural Science Foundation of China (5147127). Natural Science Foundation for Youths of Heilongjiang Province of China(QC2018064) and Training Plan of Young Innovative Talents in Colleges and Universities of Heilongjiang Province of China (UNPYSCT-2018196).

**Author' contribution** All the authors have involved equally in the realized work. Mr. Pengqiang Fu, Yan Wang, Yuhang Miao, Yiwen Wang, Mrs. Lijie Zhou, Sisi Yang: paper writing, problem formulation, approaches proposal and experimental performing and analysis.

**Availability of data and materials** The used data and materials are available when requested.

**Code availability** Not applicable.

## Declarations

**Ethical approval** The submitted work is original and has never been published elsewhere in any form or language.

**Consent to participate** Not applicable.

**Consent for publish** Not applicable.

**Conflict of interest** The authors declare no competing interests.

# References

[1] Liu D F, Tang Y, Cong W L. A review of mechanical drilling for composite laminates[J]. Composite Structures, 2012, 94(4): 1265–1279.

[2] P.J. Hazell, C. Stennett, G. Cooper. The effect of specimen thickness on the shock propagation along the in-fibre direction of an aerospace-grade CFRP laminate[J]. Composites Part A: Applied ence and Manufacturing, 2009, 40(2): 204-209.

[3] Li Shaomin et al. A self-adaption normal direction and active variable stiffness low-frequency vibration-assisted system for curved surface drilling[J]. Precision Engineering, 2020, 64(prepublish) : 307-318.

[4] Kong Linghao and Gao Dong and Lu Yong. Novel tool for damage reduction in orbital drilling of CFRP composites[J]. Composite Structures, 2021, 273.

[5] Zhang Hui, Pan Xin. Research on the accuracy calibration method of robot automatic hole making system[J]. Mechanical Science and Technology, 2020, 39(05): 815-820.

[6] Wei Wang. Study of automated hole making process with unidirectional pressing by combined action of multiple parameters[D]. Nanjing University of Aeronautics and Astronautics, 2020.

[7] Olsson T, Haage M, Kihlman H, et al. Cost-efficient drilling using industrial robots with high-bandwidth force feedback[J]. Robotics

and Computer-integrated Manufacturing, 2010, 26(1): 24-38.

[8] Von Drigalski F W H E, El Hafi L, Uriguen Eljuri P M, et al. Vibration-Reducing End Effector for Automation of Drilling Tasks in Aircraft Manufacturing[J]. IEEE Robotics and Automation Letters, Vol.2, NO.4, October 2017.

[9] Devlieg R, Sitton K, Feikert E, et al. ONCE (One-sided Cell End effector) robotic drilling system[R]. SAE Technical Paper, 2002.

[10] Bu Yin, Tian Wei, Liao Wen He. Investigation of correlation between interlayer gap and burr height in drilling of stacked Al-7475 materials[J]. Proceedings of the Institution of Mechanical Engineers, Part B: Journal of Engineering Manufacture, 2017.

[11] Hai Wei Li, Xin Pan, Hui Zhang, Jie Du, De Yi Li. Study on the application of automatic hole making technology in an aircraft assembly[J]. Aviation manufacturing technology, 2021, 64(21): 84-89+95.

[12] Wang Wei, Wang Min, Chen Wen liang. Compression force optimization considering the instantaneous springback of one-way compression of wall panels[J]. Journal of Beijing University of Aeronautics and Astronautics,2020,46(01): 210-219.

[13] Jiang Shangyang. Research on the fracture problem of particle reinforced composites based on extended finite element[D]. Jinan University, 2015.

[14] Shu-Jun Y, Yan W. Cornish-fisher expansion for probabilistic power flow of the distribution system with wind energy system[C]// 2011 4th International Conference on Electric Utility Deregulation and Restructuring and Power Technologies (DRPT). IEEE, 2011.

[15] Bi Yunbo, Li Xia, Yan Weimiao, Shen Liheng, Zhu Yu, Fang Wei. Optimization of the pressing force of the presser foot for the spiral milling hole process[J]. Journal of Zhejiang University (Engineering and Technology Edition), 2016, 50(01): 102-110+172.

[16] Wang X, Kwon P Y, Sturtevant C, et al. Tool wear of coated drills in drilling CFRP[J]. Journal of Manufacturing Processes, 2013, 15(1): 127.

[17] Li Xia. Optimization of the pressing force of the presser foot during the process of robot-automated spiral milling holes[D]. Zhejiang University, 2015.

[18] Meng Q, Zhang K, Cheng H, et al. An analytical method for predicting the fluctuation of thrust force during drilling of unidirectional carbon fiber reinforced plastics[J]. Journal of Composite Materials, 2015, 49(6): 699-711.